

SLIM (Slit Lamp Image Mosaicing): Handling Reflection Artifacts

Kristina Prokopetc^{1,2} · Adrien Bartoli²

Received: date / Accepted: date

Abstract

Purpose. The slit lamp is an essential instrument for eye care. It is used in navigated laser treatment with retina mosaicing to assist diagnosis. Specifics of the imaging set-up introduce bothersome illumination artifacts. They not only degrade the quality of the mosaic but may also affect the diagnosis. Existing solutions in SLIM manage to deal with strong glares which corrupt the retinal content entirely while leaving aside the correction of semi-transparent specular highlights and lens flare. This introduces ghosting and information loss.

Methods. We propose an effective technique to detect and correct light reflections of different degrees in SLIM. We rely on the specular-free image concept to obtain Glare-Free (GF) image and use it coupled with a contextually driven probability map to segment the visible part of the retina in every frame before image mosaicing. We then perform the image blending on a subset of all spatially aligned frames. We detect the lens flare and label each pixel as ‘flare’ or ‘non flare’ using a probability map. We then invoke an adequate blending method. We also introduce a new quantitative measure for global photometric quality.

Results. We tested on a set of video sequences obtained from slit lamp examination sessions of 11 different patients presenting healthy and unhealthy retinas. The segmentation of glare and visible retina was evaluated and compared to state-of-the-art methods. The correction of lens flare and semi-transparent highlight with content-aware blending was applied and its performance was evaluated qualitatively and quantitatively.

Conclusions. The experiments demonstrated that integrating the proposed method to the mosaicing framework significantly improves the global photometric quality of the mosaics and outperforms existing works in SLIM.

K. Prokopetc^{1,2} prokopec.kristina@mail.ru
A. Bartoli² adrien.bartoli@gmail.com

¹ Quantel Medical
11 rue du Bois Joli, 63808 Cournon-d’Auvergne, France

² EnCoV, IP, UMR 6602 CNRS / Université Clermont Auvergne
28 place Henri Dunant, 63001 Clermont-Ferrand, France

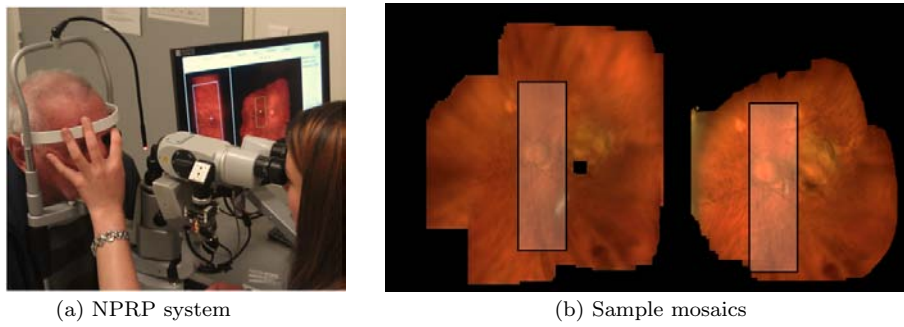


Fig. 1: Retinal image mosaicing with a slit lamp. (a) slit lamp system, developed at QuantelMedical, France and (b) sample mosaics constructed during the examination session with the slit lamp, the FOV is shown as a rectangular region. (Please, refer to the electronic version for better visualization of all figures in this paper.)

Keywords specular highlight · glare · lens flare · motion cue · context · retinal mosaicing · image blending · slit lamp

1 Introduction

Retinal examination with the slit lamp is the most important technique dating back to the 1980-ies, which remains prevalent in clinical ophthalmology nowadays. It allows the eye to be examined with a light beam or ‘slit’ whose height and width can be adjusted. The slit of light, directed at an appropriate angle, emphasizes the anatomic structures of the eye, allowing for a close inspection. It is also used for laser delivery in navigated panretinal photocoagulation (NPRP) - the standard treatment for numerous retinal diseases such as diabetic retinopathy. Currently, NPRP can be performed by computer guided systems which combine real-time imaging, pre-operative planning and intra-operative navigation [12,8,9,20]. Because the images captured with the slit lamp have a narrow field of view (FOV) visualizing only thin portions of the retina, view expansion with image mosaicing became an important part of slit lamp based NPRP systems (Fig. 1).

Obtaining a geometrically and photometrically accurate retinal mosaic is a difficult task due to the numerous challenging conditions. When performing retinal examination with a slit lamp the imaging set-up is arranged so that the axis of the observation component is nearly coaxial with the axis of the illumination component. Both are fixed on the moving base, controlled by the ophthalmologist. The light beam is focused on the retina using a hand-held direct contact lens of strong convergence (Fig. 1(a)). This essential requirement, unfortunately, introduces bothersome illumination artifacts that populate the image (Fig. 2).

The reflections of the light from the slit lamp on the cornea (the transparent layer forming the front of the eye) and the contact lens of strong convergence create specular highlights that are difficult to separate from the retina (Fig. 2(a)). Worsened by changing exposure which is adopted to the patient’s comfort, they obscure and degrade retinal details. Moreover, as they appear brighter than the

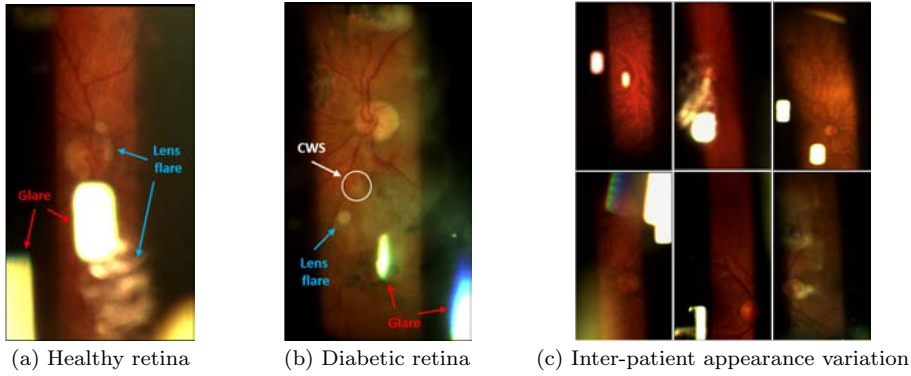


Fig. 2: Typical slit lamp images demonstrating the appearance variation of the light reflection of different origins. CWS - cotton wool spot. (Best viewed electronically.)

dominant color of the retina they may be wrongly recognized as ‘cotton wool spots’ - abnormal findings on the retina which appear as small, yellow-white (or grayish-white), slightly elevated cloud-like lesions (Fig. 2(b)). These are typical for diabetic retinopathy, hence complicating diagnosis. Reflection control during slit lamp assisted examination relies primarily on intentional vignetting and anti-reflection coatings of the contact lens. Despite this provision, the unwanted reflections still occur. Glare eliminates all information in the affected pixels and the other types of reflections can introduce artifacts in feature extraction algorithms, which are critical in our application.

In this paper we present a new methodology to overcome this issue and obtain visually consistent mosaics. We propose a two-stage solution addressing the problem of strong glares as the pre-processing step in the mosaicing pipeline while correcting lens flare and haze at the image blending stage. We also introduce a new quantitative measure for global photometric quality. Our main contribution is a SLIM dedicated method which handles different types of illumination artifacts, as opposed to existing works.

2 Related Work

2.1 Specular Highlight Correction in Medical Imaging

Automatic glare removal in colposcopy was the focus in [6]. The authors proposed a single-image technique where they used the green image component as the feature image, given its high glare to background ratio. Glare regions were detected as saturated regions by adaptive thresholding and morphological top hat filters. The watershed segmentation was then applied to find the contour of the glare regions, which were then restored using inpainting. A similar approach was presented in [13] to automatically detect and correct specular reflections in thoracoscopic images. The reported results proved both methods to be adequate on the application specific datasets. Specifically, the inpainting was acceptable due to the homoge-

neous texture of the affected regions while in SLIM this would rather produce false details than restore the ‘true’ content.

A machine learning (ML) method was successfully applied to the segmentation and tracking of surgical tools in laparoscopic videos [1]. The authors did not tackle the problem of specular highlights directly. Instead they used a random forest classifier trained with feature vectors which combine color and structural information and relied on their distinctive power. This, provided acceptable results. In [4] specular highlight segmentation was addressed as a part of ML-based organ segmentation. The specularities were found by thresholding the luminance and saturation channels in the HSV color space after Gaussian smoothing, and the binary decision was appended to the main classification framework.

Related works in SLIM [2, 12, 9] exploit intensity thresholding based segmentation of the illuminated retina using different color channels of a single RGB image. This approach is sufficient for simple video sequences where a care over reflection was taken by the ophthalmologist and the patient was not very photosensitive, resulting in reduced apparent motion. However, this is not always the case in practice and a more complex solution is necessary to achieve acceptable results. Recent work [20] employs ML with training on a manually labeled database for per-pixel classification. As in [1], the authors opted to use multiple color spaces as features, and added the spatial information. The reported results outperform those from [12] and provide robust filtering of strong specular highlights. However, as can be seen from the experimental outcomes, the significant part of the retinal content covered by semi-transparent highlight and lens flare appeared to be excluded from the mosaic, leading to a loss of valuable information.

2.2 Specular Highlight Correction in Non-medical Applications

[16] and [14] are the popular single-image generic solutions nowadays. More recent works on the subject were also presented in [18, 19, 5, 17, 7, 15]. [16] proposed a method to separate diffuse and specular reflection components using chromaticity-based iterations with regard to the logarithmic differentiation of the specular-free (SF) image using two spatially adjacent pixels. [14] separates reflections in a color image based on the error analysis of chromaticity and appropriate selection of color for each pixel by solving for the dichromatic reflection model as a least-squares problem. Both methods use the concept of SF image, which allows them to decide for specular and diffuse pixel candidates. According to our experiments (see Sect. 4.2) the direct application of their methods in SLIM is not sufficient.

A generic single-image based solution in [18] relies on the observation that the maximum fraction of the diffuse color component in local patches changes smoothly. The authors applied a low-pass filter so that the maximum diffuse chromaticity values can be propagated from the diffuse pixels to the specular pixels. Unlike other methods, this can process high-resolution images at video rate, which makes it suitable for real-time applications. In [5], similar to [16], the authors derived an SF image by applying a dark channel prior and used it along with a maximum a posteriori probability estimation to separate the specular and diffuse components. Reported results were evaluated only visually and seem to provide slightly better outcome compared to [16] and [18] but weaker in computation time.

A solution for specular removal in stereo-vision as proposed in [19], using two images to compute a vote distribution for a number of illumination chromaticity hypotheses via correspondence matching. The authors use motion cues assuming that highlights on the two images do not spatially overlap. Thus, the diffuse component of a pixel in the highlight can be recovered by finding its corresponding pixel in the other view. This assumption holds for the cases where the observation system and light source move independently from each other and the observed object remains static. In SLIM, however, a larger set of observations is necessary to recover the ‘true’ color while practically it might be possible to obtain a suitable approximation only. An analogous assumption was employed in [17, 15, 7].

2.3 What Solution for SLIM?

Most of the aforementioned single-image solutions are capable to correct strong glare. However, they share the same problem: they generally result in noticeable artifacts when applied directly in SLIM. Multi-image methods utilize the motion cues for highlight localization and correction. In SLIM, due to the specifics of the imaging set-up (see Sect. 4.1), the apparent motion of specular highlights can be noticed, but, unlike in previous work, more than two consecutive observations are required. Moreover, the limited FOV of one frame cannot capture the highlight fully. Therefore, the motion cues are useful but shall be engaged as soft constraints. Learning appearance variation from multiple images has proved to outperform simpler methods [20]. However, the inability to model complex color and intensity variation of the reflections associated with lens flare make it unsuitable for our goals in SLIM. Unlike related works, we do not limit the methodology only to correct the strong specular highlight like glare, but also lens flare patches of varying colors and shapes, and a more global haze, affecting contrast and color saturation. Our solution inherits some core ideas from [14, 18, 17, 20]. Our contribution is twofold:

- Because the generic methods applied in our application do not provide acceptable results we propose a dedicated solution to remove glare and retrieve informative retinal content in SLIM. We introduce a fast single-image technique using the concept of SF image and contextual information as the first stage of our method.
- As a second stage, we consider the correction of different types of specular highlights, unlike other methods which deal only with strong glare. We incorporate the motion cue for content-aware image blending where appropriate action is invoked to obtain a good approximation of the ‘true’ color.

3 Specular Highlight Correction for SLIM

3.1 Method Overview

We outline the proposed method in Fig. 3. This consists of two main steps: *(i)* single-image glare removal and retina segmentation and *(ii)* multi-image lens flare correction by content-aware blending. We rely on the SF image concept introduced in [16] to obtain Glare-Free (GF) image and use it coupled with contextually driven

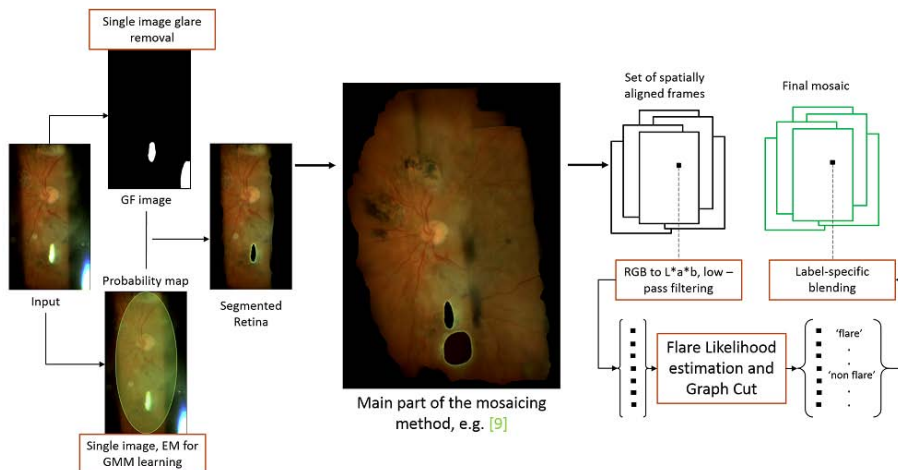


Fig. 3: Method overview. (Best viewed electronically.)

probability maps to segment the visible part of the retina at every frame before image mosaicing. For the sake of clarity we show the mosaicing block in a compact form and refer to the method developed in [9]. We then proceed directly to the image blending where a subset or all frames have been transformed and spatially aligned. We detect the lens flare areas on a set of overlapping images and label each pixel as ‘flare’ or ‘non flare’ using a probability maps. Finally, we invoke an adequate blending method.

3.2 Single-image Glare Removal and Retina Segmentation

Segmentation of the informative retinal content from slit lamp images is a challenging task. The recent work of [20] was not found to be suitable for effective retina segmentation in our datasets (see Sect. 4.2). The concept of SF image discussed in Sect.2 is just an approximation of ground truth. Nonetheless, it has been demonstrated to be effective for single-image glare removal. Incorporating contextual information is considered as one of the most effective approaches in medical applications [10]. Retinal images obtained with a slit lamp have a narrow FOV localized in the center of the image resulting in big part of the image containing dark pixels. This property can be used to obtain the region of interest (ROI) to reduce the processing load. Our approach can be summarized in the following steps:

Step 1: pre-processing. First the image is converted to the LMS (Long, Medium, and Short light wavelengths) color space. This is commonly used color space to estimate the appearance of a pixel under a different illumination. Based on the observation that the maximum fraction of the unsaturated pixels in local patches changes smoothly we proceed with low-pass filtering similar to [18] and obtain I_{LP} . We then compute $C_{min} = \frac{\min(I_{LP})}{\text{mean}(I_{LP})}$ - the maximum chromaticity image as a pixelwise division of the minimum value over three components of I_{LP} and the mean value respectively. This computation results in a binary image, where the most glare pixels have intensity equal to 1.

Step 2: informative pixel selection. Given the priors on the location of the slit in the image we filter out highly improbable locations of the informative retinal content. For each pixel in the image we compute a conditional probability of the retinal content occurring at this pixel given the center of the image \mathbf{c}_I . We model this contextual constraint with a Gaussian Mixture Model (GMM):

$$P(\mathbf{p}|\mathbf{c}_I) = \sum_{i=1}^K w_i G(\mathbf{p} - \mathbf{c}_I; \mu_i, \Sigma_i) \quad (1)$$

where K is the number of GMM components and $\{w_i, \mu_i, \Sigma_i\}$, $i = 1, \dots, K$ are the GMM's parameters estimated with Expectation Maximization (EM). The model is learned offline on a set of annotated frames from different video sequences. Here, K was empirically tuned to represent two Gaussian components. We apply the learned GMM on a test frame and obtain a probability map.

Step 3: combination. Here we incorporate the positional prior learned in the previous step to filter out uninformative areas of the image and obtain the final segmentation of retinal content. Thus, we keep \mathbf{p} as a retinal content if $P(\mathbf{p}|\mathbf{c}_I) \geq t$, where t is a probability threshold which we empirically set to 0.6. We perform logical XOR operation with the GF image mask from *Step 1* within the estimated region. This allows us to keep only those pixels for the final result where the GF mask or the estimated region, but not both, contain a nonzero element at the same location.

3.3 Multi-image Lens Flare Correction: Content-aware Blending

Localized flare patches in areas of uniform color and brightness in non-medical images can be easily corrected by copying parts of neighboring areas over the affected area. The situation is much more complicated when the flare affects areas with lots of detail and tonal variations as retinal content. Correction is generally not possible without knowing beforehand what the affected areas should look like in the absence of flare. This requires a sophisticated per-pixel analysis in different views. Given a set of spatially aligned images we want to detect which pixels are likely to be pixels affected by lens flare. Once the lens flare regions are revealed, their visibility may be corrected by performing an adequate color mapping. The procedure is as follows:

Step 1: pre-processing. Because reflection caused by lens flare has a complicated nature it is necessary to address the problem within an appropriate color space representation. Thus, for a given pixel on the mosaic $M(\mathbf{q})$, a set of overlapping frames are first transformed to the L^*a^*b color space. Following the same reasoning as described in the *step 1* of section 3.2, we apply an image guided filter to the L component. Because the L component represents scene luminance and low-pass filtering adjusts the local intensity to its neighbors it is more likely to obtain well preserved boundaries of areas affected by lens flare.

Step 2: flare detection from color. Because regions affected by lens flare have specific colors, which are different from the rest of the retina, it motivates the use of color GMMs. We learn a simple GMM similarly to [4] offline on a set of

manually annotated images where the pre-processing from the previous step was applied:

$$P(\mathbf{l}|\lambda) = \sum_{i=1}^K w_i G(\mathbf{l}; \mu_i, \Sigma_i) \quad (2)$$

with $K = 3$ Gaussian components. Here \mathbf{l} is the image pixel and $\lambda = \{w_i, \mu_i, \Sigma_i\}$, $i = 1, \dots, K$ are the GMM's parameters estimated with EM. We obtain a probability map for every L component in the observation set of frames on the mosaic using the trained GMMs. This indicates the probability that a given pixel in the observation belongs to the flared region. We use a Graph Cut algorithm [3] to mark the pixel as 'flare' or 'non flare'. As this is posed as a binary labeling problem, the Pott's Energy function is sufficient:

$$E(I) = \sum_{\mathbf{p} \in S} |I_{\mathbf{p}} - I'_{\mathbf{p}}| + \sum_{\mathbf{p}, \mathbf{q} \in N} K(\mathbf{p}, \mathbf{q}) T(I_{\mathbf{p}} \neq I_{\mathbf{q}}) \quad (3)$$

where $I = \{I_{\mathbf{p}} | \mathbf{p} \in S\}$ are the unknown 'true' labels over the set of pixels S and $I' = \{I'_{\mathbf{p}} | \mathbf{p} \in S\}$ are the observed labels. The Potts interaction is specified by $P(\mathbf{p}, \mathbf{q})$, which are the penalties for label discontinuities between adjacent pixels. The function T is an indicator function. This is optimally solved by a single execution of max-flow.

Step 3: blending. We count the number of pixels belonging to each label and identify the majority. We take the average luminance L of the majority as a L_t - *top luminance* and the average of the rest of the pixels as a L_b - *bottom luminance*. We then invoke an appropriate mapping function. This is inspired by [11]. Thus, if the majority is 'flare' pixels we apply 'color burning' - divide the inverted L_b by the L_t , and then invert the result as $C_{burn} = 1 - (1 - L_b)/L_t$. This darkens the L_t increasing the contrast. In the opposite case we apply 'color dodging' - divide the L_b by the inverted L_t such as $C_{dodge} = L_b/(1 - L_t)$. This lightens the L_b depending on the value of the L_t .

4 Experiments and Results

4.1 Dataset and Evaluation Strategy

The datasets used for evaluation were obtained from slit lamp examination sessions performed on 11 different patients at University Hospital of Saint-Étienne, France, presenting healthy and unhealthy retinas. The NPRP system developed at QuantelMedical was used. The videos were captured with a CCD camera at 60fps were 2-3 minutes long. The proposed glare removal and retina segmentation were evaluated on a set of 270 manually annotated image frames sampled from the set of videos. This was to ensure the coverage of patient-specific and lens-specific specular highlight variation. The images were annotated with binary masks to separately assess the performance of glare removal and retina segmentation. The proposed blending technique for lens flare correction was rated on a set of geometrically aligned video frames obtained by the method described in [9]. Further details along with experimental results are provided next.

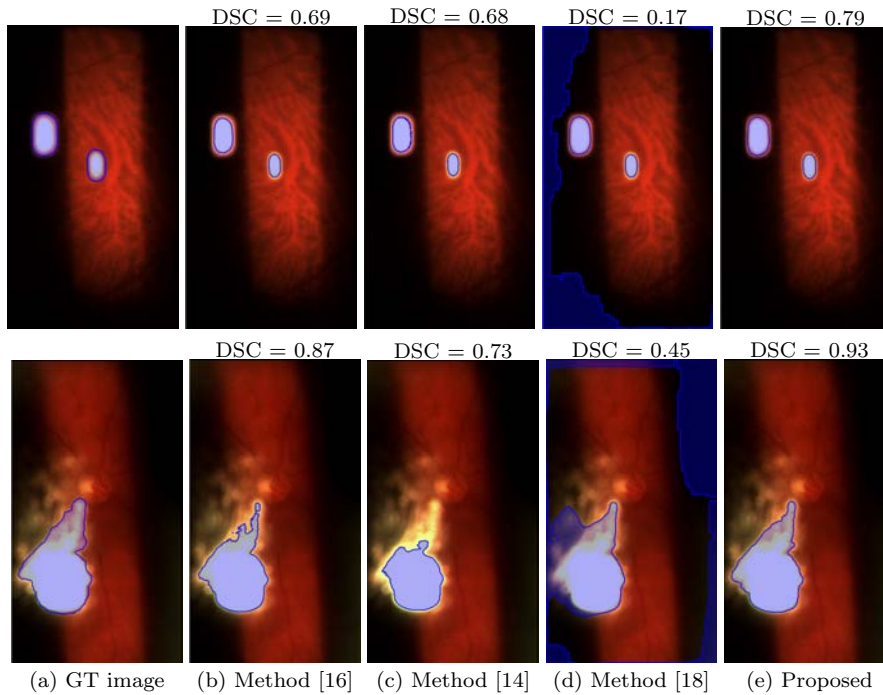


Fig. 4: Comparative results of glare removal. GT - Ground Truth. Example of a simple case is shown in the first row and the second row illustrates more complicated condition. (Best viewed electronically.)

4.2 Single-image Glare Removal and Retina Segmentation

We start with the comparison of our glare removal technique with the existing methods [16, 14, 18]. We manually annotated selected datasets by drawing the contour around regions obscured by highly saturated pixels. In simple cases, where the patient appeared to be less photosensitive and the image acquisition was not polluted by mixture of different degrees of reflections the glared region boundaries were easy to locate. Because most of the time it is difficult to observe a clear boundary between a glared region and the surrounding distorted areas, we opted for a middleground. The results for such two cases are shown in Fig. 4.

We computed the Dice Similarity Coefficient (DSC) to assess the similarity with the annotated regions. The higher the value the more similar the algorithm's output to the reference mask. For the simple case (Fig.4(first row)) all the methods perform well while in the difficult case (Fig.4(second row)) only the proposed method provides acceptable results.

We then combine the GF image with the spatial probability map to obtain the visible retinal content. The experimental results of our method compared to the simple thresholding technique used in [9] and the ML-based approach proposed in [20], are illustrated in Fig. 5. Here we also compute statistical measures for every output and average it over results on 270 annotated samples as shown in Table 1. One can see that our method provides higher values indicating better performance.

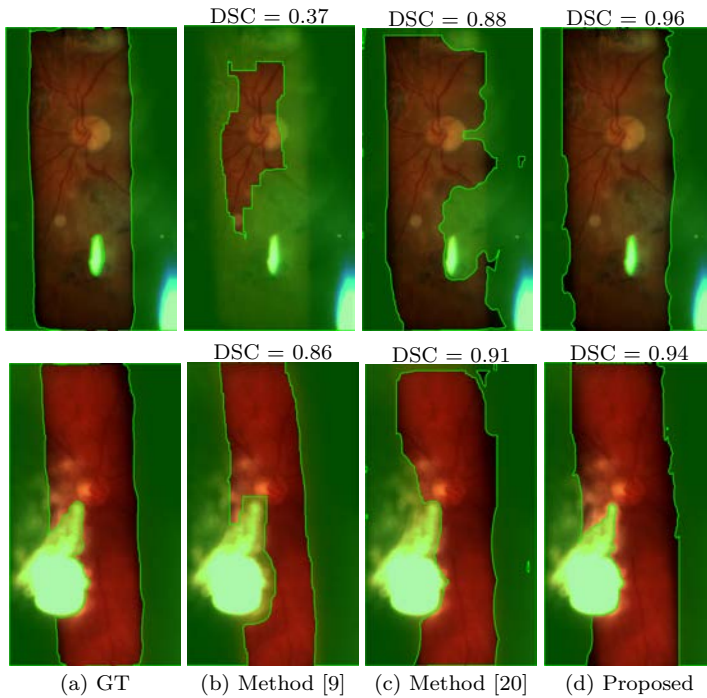


Fig. 5: Comparative results of retinal content segmentation. GT - Ground Truth. (Best viewed electronically.)

	Precision	Accuracy	Specificity	Sensitivity
Method [9]	0.30	0.70	0.58	0.86
Method [20]	0.90	0.92	0.94	0.89
Proposed	0.92	0.95	0.97	0.90

Table 1: Retinal content segmentation performance.

4.3 Multi-image Highlight Correction: Content-aware Blending

The most traditional way to evaluate the photometric quality of slit lamp image mosaics is still based on the visual assessment of ophthalmologists. Even though the experts' opinion is a good reference it is a subjective evaluation which may differ between experts and may prevent the mosaic from being used. Here we propose a new quantitative evaluation of the global photometric quality. We propose to use a Blending Consistency Measure (BCM). It assesses the quality of the blending by computing the standard deviation of a pixel's intensity in the transformed image $I(\mathbf{q})$ from a set of corresponding locations in the mosaic $M_i, i = 1, 2, \dots, n$ as:

$$BCM = \sqrt{\frac{1}{n-1} \sum_{i=1}^n |I(\mathbf{q}) - \mu|^2} \quad , \quad \text{where} \quad \mu = \frac{1}{n} \sum_{i=1}^n M_i \quad (4)$$

The results shown in Fig. 6 (see next page) demonstrate one of the mosaics for visual assessment. We take the mosaicing result obtained by the modified version of the method in [9] where we removed the illumination correction (Fig.6(a)). We then compute BCM for this uncorrected mosaic and the results obtained with the inclusion of the correction techniques from existing works in SLIM ((Fig.6(b), (c)) and the proposed method (Fig.6(d)). The computed metric spans the range [0;255]. We show the computed results represented as a percentage value. The smaller the value, the better the blending consistency. The mosaic in Fig.6(c) consists of 530 frames while Fig.6(a), Fig.6(b) and Fig.6(d) are made of 212 frames as they are based on the mosaicing method [9] which uses key-frames. As can be noticed, the mosaic in Fig.6(c) appears darker than others. This is due to the blending method used in [20], where the intensity fades toward the border of the segmentation mask which we have re-implemented strictly following the provided formulas.

One can see that the proposed method significantly improves the global photometric quality of the mosaic in the major areas and outperforms existing works. This is true for the majority of the cases in our dataset. However, it does not work well in the lower right corner of the illustrated example (Fig. 6(d)). Our glare removal part was specifically designed to work for a middleground and keep as much more valuable information as possible. Thus, it is not always able to erase all the glare-like artifacts but it always keeps the ‘uncorrupted’ retina. [20], in the other hand, does not include the mentioned region (Fig. 6(c)) and, according to the experiments on other sequences, it cuts out a big part of the retinal content which is not corrupted by artifacts and can be useful for diagnostic purposes. This complication may be due to various reasons: different contact lenses were used in the procedure, the manual navigation by an ophthalmologist is not always precise, and the industrial prototype we use is constantly under development and it is not perfect. The improvement we expect to achieve in future work will mainly come from the improvement of the prototype itself.

5 Conclusion

In this paper we showed how to segment the informative part of the retinal content and correct specular highlights of different degrees in SLIM. To this end we studied several specular highlight removal and correction approaches proposed in the medical and non-medical domains and designed our own solution specifically adapted to our task. Firstly, we improve on the previous works by proposing a fast single-image technique to remove glares and segment the visible retina using the concept of specular-free image and contextual information. Secondly, we incorporate the notion of the type of specular highlight and motion cue for intelligent image blending. Our experimental results showed that the proposed methodology exhibits a good efficiency, significantly outperforming related works in SLIM.

6 Disclosures

Conflict of Interest: The authors declare that they have no conflict of interest.
Ethical approval: All procedures performed in studies involving human participants were in accordance with the ethical standards of the institutional and/or

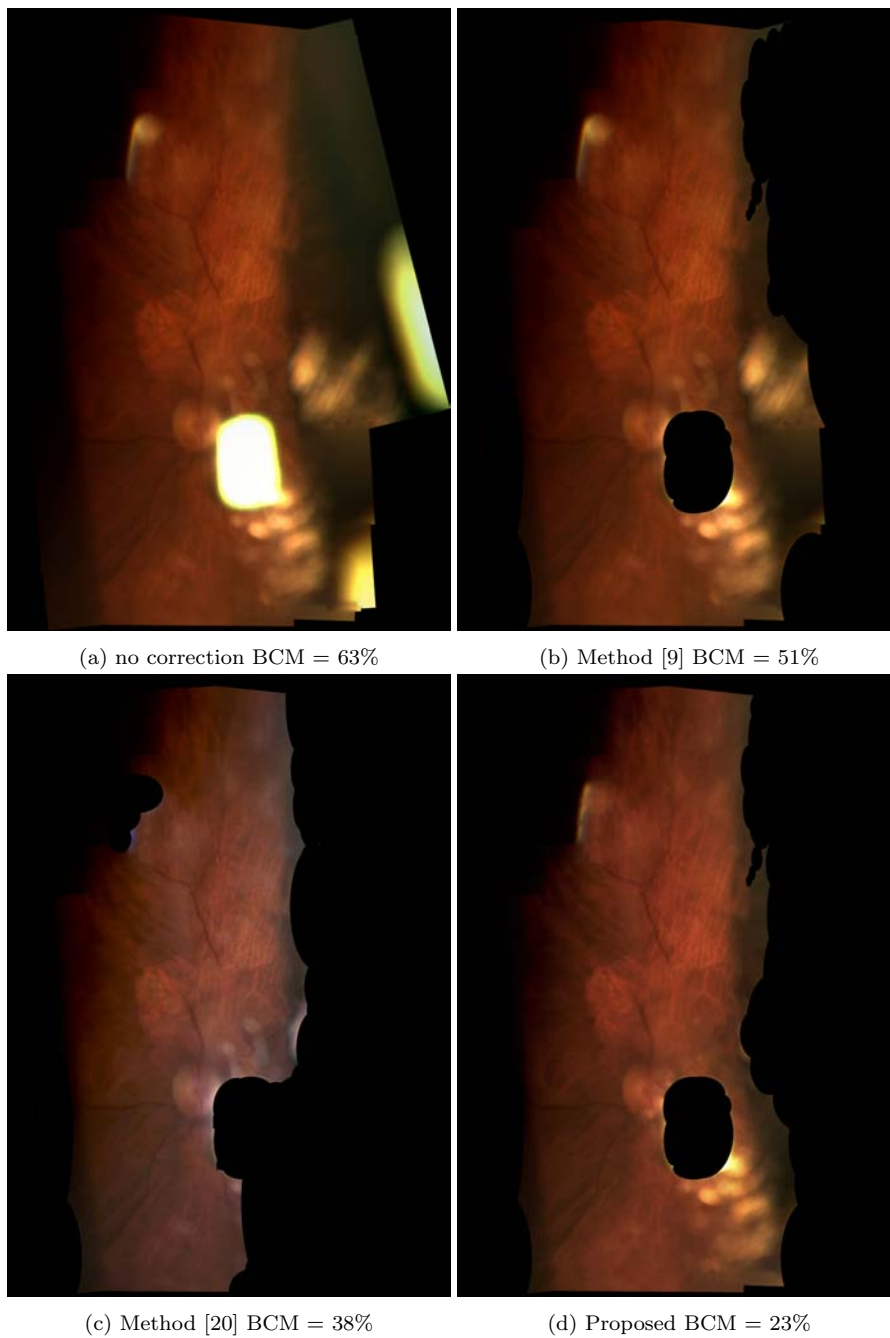


Fig. 6: The comparative results for one of the mosaics. (Best viewed electronically.)

national research committee and with the 1964 Helsinki declaration and its later amendments or comparable ethical standards.

Informed consent: Informed consent was obtained from all individual participants included in the study.

References

1. Allan, M., Ourselin, S., Thompson, S., Hawkes, D.J., Kelly, J., Stoyanov, D.: Toward detection and localization of instruments in minimally invasive surgery. *IEEE Transactions on Biomedical Engineering* **60**(4), 1050–1058 (2013)
2. Asmuth, J., Madjarov, B., Sajda, P., Berger, J.W.: Mosaicking and enhancement of slit lamp biomicroscopic fundus images. *British J. of Ophthalmology* **85**(5), 563–565 (2001)
3. Boykov, Y., Jolly, M.P.: Interactive organ segmentation using graph cuts. In: *International Conference on Medical Image Computing and Computer-Assisted Intervention*, pp. 276–286. Springer (2000)
4. Chhatkuli, A., Bartoli, A., Malti, A., Collins, T.: Live image parsing in uterine laparoscopy. In: *2014 IEEE 11th International Symposium on Biomedical Imaging (ISBI)*, pp. 1263–1266. IEEE (2014)
5. Kim, H., Jin, H., Hadap, S., Kweon, I.: Specular reflection separation using dark channel prior. In: *Proceedings of the IEEE Conference on Computer Vision and Pattern Recognition*, pp. 1460–1467 (2013)
6. Lange, H.: Automatic glare removal in reflectance imagery of the uterine cervix. In: *Medical Imaging*, pp. 2183–2192. International Society for Optics and Photonics (2005)
7. Nussberger, A., Grabner, H., Van Gool, L.: Robust aerial object tracking in images with lens flare. In: *2015 IEEE International Conference on Robotics and Automation*, pp. 6380–6387. IEEE (2015)
8. Prokopetc, K., Bartoli, A.: A comparative study of transformation models for the sequential mosaicing of long retinal sequences of slit-lamp images obtained in a closed-loop motion. *Int. J. of Computer Assisted Radiology and Surgery* pp. 1–10 (2016)
9. Prokopetc, K., Bartoli, A.: Reducing drift in mosaicing slit-lamp retinal images. In: *The IEEE Conference on Computer Vision and Pattern Recognition (CVPR) Workshops*, pp. 93–100. IEEE (2016)
10. Prokopetc, K., Collins, T., Bartoli, A.: Automatic detection of the uterus and fallopian tube junctions in laparoscopic images. In: *International Conference on Information Processing in Medical Imaging*, pp. 552–563. Springer (2015)
11. Reinhard, E., Stark, M., Shirley, P., Ferwerda, J.: Photographic tone reproduction for digital images. *ACM Transactions on Graphics* **21**(3), 267–276 (2002)
12. Richa, R., Linhares, R., Comunello, E., von Wangenheim, A., Schnitzler, J.Y., Wassmer, B., Guillemot, C., Thuret, G., Gain, P., Hager, G., et al.: Fundus image mosaicking for information augmentation in computer-assisted slit-lamp imaging. *IEEE transactions on medical imaging* **33**(6), 1304–1312 (2014)
13. Saint-Pierre, C.A., Boisvert, J., Grimard, G., Cheriet, F.: Detection and correction of specular reflections for automatic surgical tool segmentation in thoracoscopic images. *Machine Vision and Applications* **22**(1), 171–180 (2011)
14. Shen, H.L., Zhang, H.G., Shao, S.J., Xin, J.H.: Chromaticity-based separation of reflection components in a single image. *Pattern Recognition* **41**(8), 2461–2469 (2008)
15. Sun, C., Liu, S., Yang, T., Zeng, B., Wang, Z., Liu, G.: Automatic reflection removal using gradient intensity and motion cues. In: *Proceedings of the ACM on Multimedia Conference*, pp. 466–470. ACM (2016)
16. Tan, R.T., Ikeuchi, K.: Separating reflection components of textured surfaces using a single image. *IEEE transactions on Pattern Analysis and Machine Intelligence* **27**(2), 178–193 (2005)
17. Xu, C., Wang, X., Wang, H., Zhang, Y.: Accurate image specular highlight removal based on light field imaging. In: *Visual Communications and Image Processing*, pp. 1–4. IEEE (2015)
18. Yang, Q., Wang, S., Ahuja, N.: Real-time specular highlight removal using bilateral filtering. In: *European Conference on Computer Vision*, pp. 87–100. Springer (2010)
19. Yang, Q., Wang, S., Ahuja, N., Yang, R.: A uniform framework for estimating illumination chromaticity, correspondence, and specular reflection. *IEEE Transactions on Image Processing* **20**(1), 53–63 (2011)
20. Zanet, S., Rudolph, T., Richa, R., Tappeiner, C., Sznitman, R.: Retinal slit lamp video mosaicking. *Int. J. of Computer Assisted Radiology and Surgery* pp. 1–7 (2016)